ChemElectroChem

Concept
doi.org/10.1002/celc.202400659

Chemistry Europe
European Chemical Societies Publishing

www.chemelectrochem.org

High-Entropy Halides for Intercalation Battery Electrode Materials

Sebastian Schumacher,*[a, b] Evgeny V. Alekseev,*[a] Shicheng Yu,*[a] Hermann Tempel,[a] and Rüdiger-A. Eichel[a, b, c]

The potential use of high-entropy materials in batteries has recently attracted considerable interest. Compared to traditional materials, high-entropy materials exhibit a high defect density and degree of internal entropy, resulting in enhanced ion storage capabilities, ionic conductivity, and electrochemical stability. High-entropy oxides represent a more extensively investigated material for various electrochemical applications, particularly for potential use as a cathode or electrolyte in battery applications. These multicomponent systems are distinguished by their structural complexity and exhibit enhanced cycling stability, exceeding the performance of traditional oxide materials. The exploration of high-entropy halides as electrode materials is less extensive than that of their traditional counterparts, despite the latter being the subject of considerable research. This work offers a concise overview of how high-entropy materials can be applied to halide phases, focusing on the transition from high-entropy oxides to high-entropy halides.

Introduction

High-entropy materials (HEMs) comprise a singular crystal lattice in which multiple elements (typically transition metals) occupy the same sites on the crystal lattice. In light of these characteristics, these phases can be regarded as highly intricate solid solutions. The concept was initially introduced in 2004[1,2], and has since been employed extensively in metallurgy, where such high-entropy alloys achieve exceptional resistance against corrosion and an overall increased wear resistance.[3] Since 2015, the high-entropy concept has been applied to oxides for ceramic applications,[4] and subsequently to oxyhalide[5] and fluoride perovskites[6] electrode materials in batteries.[5–6] The high-entropy concept was initially applied to ceramic oxides, resulting in [CoCuMgNiZn]O[4] and it was concluded that configurational entropy is maximized if an equimolar stoichiometry is used, promoting the formation of single-phase high-entropy oxides (HEOs).

For high-entropy ceramics, there is a broad array of possible materials, such as oxides, borides, nitrides, hydrides, carbides, oxynitrides and silicides.[7] These materials have a multitude of highly desirable properties like overall lower thermal conductivity when compared to traditional ceramics, increased thermal stability, and various electrical properties to be used as, for example, exceptional piezoelectric materials or their optoelectronic properties, allowing them to be implemented in a multitude of fields of application such as photovoltaic, microelectronics or thermoelectrics.[7]

Subsequently, the high-entropy concept was extended to other chemical systems and fields of applications, including developing materials for electrochemical applications such as a high-entropy oxide perovskite with a composition of [((Bi, Na)$_{0.2}$(La, Li)$_{0.2}$ (Ce, K)$_{0.2}$Ca$_{0.2}$ Sr$_{0.2}$]TiO$_3$, which was used as an anode material for lithium-ion batteries (LIBs).[8] A series of solid solutions combining perovskite oxides with perovskite fluorides resulting in $(Ba_{0.5}Sr_{0.5}Co_{0.8}Fe_{0.2}O_{3-\delta})_{3/4}[K(MgMnFeCoNi)F_3]_{1/4}$ with enhanced catalytic performance in oxygen evolution reaction[5] at the initial operation. The obtained solid solutions have attractive features, such as highly mixed oxide–fluoride BX_6 octahedrons with different elements and valences, uniform element distributions, and single-phase crystalline structures, contributing to an ultrahigh S_{config}.[5]

High-entropy rocksalt oxyfluorides, such as $Li_{1.3}Mn_{0.2}Mn_{0.2}Ti_{0.1}Nb_{0.2}O_{1.7}F_{0.3}$[9] are used as cation-disordered rocksalt cathodes in which the Li^+ travels through a percolating network of 0-TM (transition metal) clusters. Various high-entropy chloride perovskites like K[MgMnCoNiZn]Cl$_3$[6] or K[MgMnFeCoNi]Cl$_3$[6] can be synthesized with a liquid synthesis approach. The resulting fluoride perovskites show increased electrocatalytic activity as electrode materials for the oxygen evolution reaction at initial operation compared to commercially available IrO_2. While there are currently no high-entropy chlorides with application for

[a] S. Schumacher, Dr. E. V. Alekseev, Dr. S. Yu, Dr. H. Tempel, Prof. Dr. R.-A. Eichel
Institute of Energy Technologies – Fundamental Electrochemistry (IET-1)
Forschungszentrum Jülich
Wilhelm-Johnen-Straße, 52428 Jülich, Germany
E-mail: s.schumacher@fz-juelich.de
e.alekseev@fz-juelich.de
s.yu@fz-juelich.de

[b] S. Schumacher, Prof. Dr. R.-A. Eichel
Material and Processes of Electrochemical Energy Storage and Conversion
RWTH Aachen University
Templergraben 55, 52062 Aachen, Germany
E-mail: s.schumacher@fz-juelich.de

[c] Prof. Dr. R.-A. Eichel
Institute of Energy Materials and Devices – Helmholtz Institute Münster: Ionics in Energy Storage (IMD-4/HI MS)
Forschungszentrum Jülich, 48149 Münster, Germany

cathode materials for batteries, two promising candidates as cathode materials would be based on Li_2MnCl_4[10] and Li_2FeCl_4.[11] These two materials show good cycling stability against lithium while having low production costs. Both potential cathode materials crystallize in $Fd\bar{3}m$ cubic anti-spinel structure and can be considered the basis for high-entropy halide (HEHs) spinel-type materials. Additionally, halide spinel halide structures such as Li_2FeCl_4 were found to have good ionic conductivities.[12] Additionally, HEOs and possibly, to an extent, HEHs could be applied as potential electrode materials for sodium-ion batteries (SIBs), as medium-entropy materials are already being applied as electrode materials for SIBs. The advantage of SIBs over LIBs would be a considerably lower production. The wide selection of possible stoichiometries and composition of HEMs allows to deeply investigate and tailor various desirable properties for any current field of application.[13]

In this work, we elaborate on high-entropy halides based on oxides and a few existing fluorides, which may be applicable as electrode materials. Specifically, after introducing the fundamentals of HEMs, synthetic and handling approaches, analytical methods, and potential applications as electrodes of HEHs are discussed.

Fundamentals of High-Entropy Materials

As shown in Figure 1, HEMs are defined by four significant properties: A high configurational entropy, severe crystal lattice distortion, diffusion effects, and so-termed cocktail or composite effects.[14] The configurational entropy can be expressed by Equation 1[1415]

$$S_{config} = -R\left[\left(\sum_{i=1}^{n} x_i \ln x_i\right)_{cation\ site} + \left(\sum_{i=1}^{m} x_i \ln x_i\right)_{anion\ site}\right] \quad (1)$$

where R is the ideal gas constant and x_i is the molar ratio of a component. A material belongs to high-entropy phases if a configurational entropy S_{config} is 1.61R or higher is achieved. Phase separation is preferred for a positive enthalpy of mixing in Equation 2. The formation of intermetallic phases is preferred for a large negative enthalpy of mixing. For the formation of single-phase HEMs, the configurational entropy must be positive, while the enthalpy of mixing must be slightly negative in Equation 2.[16]

$$\Delta G_{mix} = \Delta H_{mix} - T\Delta S_{config} \quad (2)$$

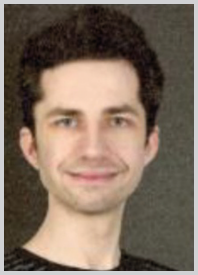

Sebastian Schumacher is a PhD student at Forschungszentrum Jülich in Germany. His research focuses on synthesizing, characterizing, and applying novel High-energy halides as electrode materials for batteries. His M.Sc. was acquired in collaboration with DLR at the University of Cologne on synthesizing and characterizing titanium dioxide aerogels using sol-gel processes.

Dr. Evgeny V. Alekseev received a diploma with Honors in Chemistry (2002) and PhD (2004) from the Lobachevsky State University. In 2005, he moved to the University of Kiel to work in synthetic materials and structural chemistry of heavy elements. Since 2011, he has been a research scientist/group leader at the Forschungszentrum Julich. His research is mainly focused on solid-state chemistry of new materials for electrochemical, catalytic, and nuclear applications. Author/co-author of more than 150 papers in this field.

Dr. Shicheng Yu was awarded his Ph.D. in chemistry from RWTH Aachen University in 2017. From 2017 to 2020, he held the postdoctoral researcher position and was later appointed senior scientist at the Institute of Energy Technologies (IET-1), Forschungszentrum Jülich in 2021. His current research primarily focuses on developing and comprehending the fundamentals governing materials and devices in energy systems.

Dr. Hermann Tempel received his PhD in chemistry from TU Darmstadt in 2013. Following a three-year postdoctoral period, he was promoted to the role of group leader, overseeing teams engaged in CO_2 electrolysis and battery development at the Institute of Energy Technologies (IET-1), Forschungszentrum Jülich. In 2022, he was appointed Head of the Functional Materials and Components Department, responsible for gas separation, material development, and system testing for batteries and electrolyzers.

Prof. Eichel studied Physics at the University of Cologne, received his doctorate from the Swiss Federal Institute of Technology (ETH) in Zurich and obtained his habilitation thesis in physical chemistry from the Technical University of Darmstadt. In 2012, he was appointed full professor at RWTH Aachen University and simultaneously acts as scientific director of the Institute of Energy Technologies (IET-1) at Forschungszentrum Jülich.

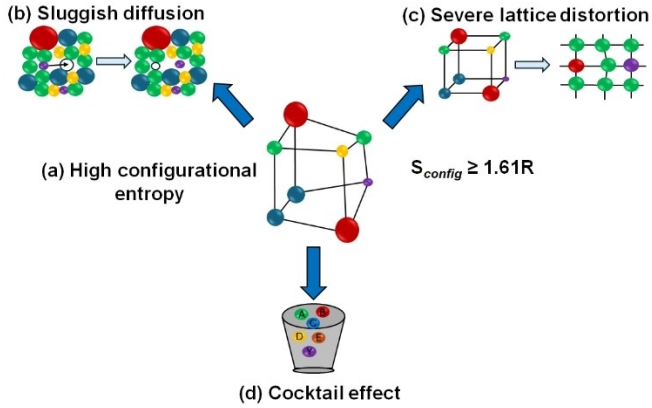

Figure 1. The four fundamental effects found within high-entropy materials: (a) high configurational entropy, (b) sluggish diffusion effects due to size mismatches of components, (c) severe lattice distortion due to size mismatches of elements, (d) cocktail effects which are unexpected synergies of different elements. Different transition metals are represented with different colors.

Different structure types can be used for the design of HEM phases. HEOs and fluorides have been reported to be synthesized in rocksalt,[9] fluorite,[17] perovskite[18] and spinel[19] structure types, as shown in Figure 2. Depending on cation size, oxidation states and synthetic parameters, a variety of HEM phases can be obtained within these classical structure types.[14,20–22]

The structural types in question exhibited significant lattice distortion and diffusion effects, which resulted from cation or anion size mismatches, preferred coordination, and spin states

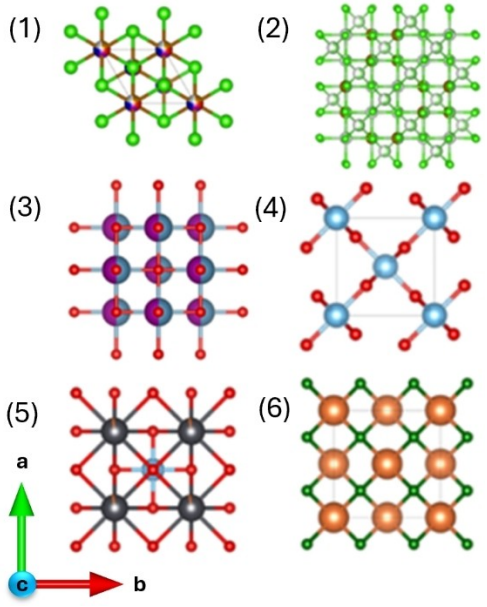

Figure 2. Crystal Structure types of common oxides, fluorides, and chlorides are potential target structures for high-entropy materials oriented along the *c*-axis. 1) $CdCl_2$-type high-entropy chloride:[17] Green = Cl, multicolored = Co, Fe, Mn, Ni, V. 2) Spinel-type Li_2FeCl_4:[26] Green = Cl, white = Li, brown = Fe. 3) Rocksalt-type CaMnO:[27] Red = O, blue = Ca, purple = Mn. 4) Rutile-type:[28] Red = O, blue = Ti. 5) Ca-doped $PbTiO_3$(perovskite-type):[29] Red = O, blue = Ti, orange = Ca, black = Pb. 6) CaF_2 (fluorite):[30] dark green = F, orange = Ca.

within a multi-component system. This can result in an increase or shortening of bond lengths between transition metals and anions, a variation in the dimensions of the unit cell, or a change in the symmetry expressed by a shift in the space group. The impact of significant lattice distortion can be observed in numerous essential material properties, including magnetism, electrochemical activity, electrochemical stability, and catalytic activity.[5–6,16,19] Furthermore, crystallographically distinct sites occupied by a range of elements (e.g., d-metals) can be partially substituted by alkali metal cations, resulting in enhanced ion mobility. This phenomenon has been observed in perovskite[23] and garnet structures[24,25]. Lastly, cocktail or composite effects describe a multitude of synergistic effects resulting from the mixing of certain cations in specific molar ratios within a single crystal lattice, which leads to an enhancement of material properties.[14]

A challenge inherent to HEMs comprising multiple components is the formation of secondary phases alongside the primary product, resulting from the multitude of potential reaction pathways in such a complex system. Even minor discrepancies in the stoichiometry and composition of a heterogeneous ensemble of materials (HEM) can result in markedly disparate material properties.[9,18,31–33]

To mitigate the formation of multiple phases, the ion size of the cations occupying the same sublattice in a HEM is ideally similar to one another, which is a standard requirement for the formation of solid solutions.[21] Due to a small Shannon ionic radius of oxygen, higher oxidation state and broader possible coordination numbers,[34] oxides usually have greater structural diversity than halides. Except for fluorides, halides exhibit considerably larger Shannon ionic radius and demonstrate reduced flexibility concerning their preferred coordination number. The predominant coordination numbers observed for these compounds, while potentially more variable for high-entropy phases due to lattice distortion and cocktail effects, are IV or VI for the metal centers and VI for the halide anions. This results in an increased unit cell size in metal halides when compared to oxides, which are prone to the formation of structural defects. The latter phenomenon is frequently observed in halide-type spinels, for instance, Li_2FeCl_4.[26] Additionally, the shift in the oxidation state of the anion from -II in oxides to -I in halides influences the stoichiometry and oxidation states of metal cations. Table 1 summarizes the differences between various anions regarding the oxidation state, Shannon ionic radius, and possible coordination numbers.

The shift to more regular (octahedral VI) coordination numbers and increased Shannon ionic radius for non-fluoride halide elements is especially notable for stabilizing perovskite and spinel-type structures. These two structural types are well known to accept different transition metals in octahedral sites, allowing complex composition and partial doping. The limits for the occupation of octahedral sites can be described by the so-called structure tolerance factors τ found within Equation 3[35] and 4.[36]

Table 1. The evolution of oxides towards halides is based on the oxidation state, Shannon radius [24], and possible coordination for these elements.

Anion	Oxidation state	Shannon Ionic Radiu (Å)	Possible coordination numbers[a]
Oxide	−2	1.40	II, III, IV, ***VI***, VIII
Sulfide	−2	1.84	***VI***
Selenide	−2	1.98	***VI***
Fluoride	−1	1.33	II, II, IV, ***VI***
Chloride	−1	1.81	***VI***
Bromide	−1	1.96	***VI***
Iodide	-1	2.2	***VI***

[a] the preferred coordination number for chalcogenide and halide elements is highlighted in bold italics.

$$\tau_{Perovskite} = \frac{R_A + R_X}{\sqrt{2}(R_B + R_X)} \quad (3)$$

$$\tau_{Spinel} = \frac{\sqrt{3}(R_B + R_X)}{2(R_A + R_X)} \quad (4)$$

Equation 3[35] describes the Goldschmidt tolerance factor for perovskite-type structures, while Equation 4[36] describes the tolerance factor for spinel-type structures. Ideally, the respective tolerance factors for perovskite and spinel structures should be 0.9 to 1.1. The exchange of oxygen for chlorine would alter the oxidation state of the transition metal from IV to II, while the alkaline earth metal cation would have to be replaced with an alkali metal cation, changing the oxidation state on the A site from II to I. Furthermore, the ionic radii of each cation would increase as well. This structure can be described as ABX_3, where B is a divalent (transition) metal and A is an alkali metal. These phases exhibit structural similarities but display disparate material properties, rendering them suitable for applications such as electrocatalysis or battery materials. The nature of the alkali- and d-metal cations plays a pivotal role in determining the suitability of these phases for such applications.[37]

Although structural similarities between halide and oxide structures are evident, the physicochemical properties of halides can diverge significantly from those of oxides. Furthermore, the methodologies employed for their synthesis and the techniques utilized in materials handling are markedly disparate, particularly due to the pronounced hygroscopic nature of halides. This results in the necessity of selecting distinct precursors for HEHs, as using the oxide analogs as starting materials is not feasible.

Synthetic and Handling Approaches of High-Entropy Halides

HEHs have some considerable differences in synthesis methods and handling compared to HEO. HEOs can usually be synthesized by traditional solid-state methods in which a mixture of precursor powders is treated by high-energy ball milling followed by subsequent calcination at appropriate temperature and time parameters[4,38]. The temperature needed for forming HEOs depends highly on the target phase but is commonly found in ranges of 400–1100 °C while using ceramic crucibles.[38] Like temperature, time parameters are often adjusted to the target phase and commonly found within 48–72 hours for calcination processes.

The rate of cooling can have a significant impact on the resulting material. Rapid cooling can result in the formation of glass phases, while slow cooling rates can result in phase separation.[16] The choice of precursors for HEOs is broad; oxides themselves, carbonates, carboxylates, acetates, and acetylacetonates are suitable for HEO synthesis as they either are stable oxides or decompose into stable oxide phases. HEOs are commonly found to be air-stable and can be safely stored normally iin ambient atmosphere, which greatly increases the convenience of use and eases potential application and analysis. HEHs, as most halide precursors, are highly sensitive to air moisture,[39] therefore, it is necessary to use moisture-protected conditions (e.g., glovebox or cleanroom). Similarly, any analytical preparation would have to be conducted under an inert atmosphere, which can result in more difficulties in characterizing and studying the resulting HEH materials.

For HEHs, traditional solid-state synthesis approaches are also applicable, but with some notable modifications to the calcination process. One such modification is that the calcination temperatures must be adjusted to a lower temperature range from 300 °C to 700 °C. The lower temperature range is chosen because the halide precursors can undergo partial decomposition processes at higher temperatures, such as $CuCl_2$.[40] An argument can be made that a HEH requires a narrow temperature range to achieve single-phase solid solutions. To achieve a fully crystallized product, longer dwelling times may be considered as a higher temperature may lead to partial decomposition, and any adjustment to cooling rates may result in either vitrification in high cooling rates or phase separation in case of low cooling rates similar to HEO materials. An advantage of halide precursors is that they frequently have low melting points, the most notable of which are $ZnCl_2$ (300 °C) and $PbCl_2$ (499 °C).[41,42] The low melting points of halide precursors can be advantageous because they can act as a flux material that effectively dissolves other solid-state precursors. This results in a more thorough and homogenous distribution of metal cations in the resulting HEHs. Low melting points could also allow for the growth of larger HEHs single crystals suitable for neutron diffraction, which would be helpful for structural analysis, especially if small cations such as Li^+ were incorporated into the structure.

Calcination times for HEHs can be considerably shorter when compared to HEOs, ranging from 24 to 48 hours, as many precursors melt at the target temperature ranges of 400 °C to 600 °C, acting as a flux. Another consideration due to the low melting points of halide precursors is the high reactivity of their melts. It leads to a strongly limited crucible material choice where a standard ceramic crucible (made of Al_2O_3 or ZrO_2) may react with the molten halide salts, forming oxyhalides or

secondary metal oxides[43] leading to impurities in the resulting HEHs. Chemically inert crucibles, such as glassy carbon or platinum, prevent reactions with salt melts and may have to be used for HEH syntheses. All calcination processes must be conducted in an inert atmosphere because an ambient atmosphere can form oxides, and a reductive atmosphere can form hydrogen halides such as HCl or HBr. Halide precursors, e.g., $CoBr_2$, $CoCl_2$, $FeBr_2$, $FeCl_2$, or $MnCl_2$, and resulting HEHs are hygroscopic and must be handled in inert conditions for preparation, synthesis, and analysis. In addition, preheating is required to remove possible hydrates for some of the starting materials like $MnCl_2$ and $FeCl_2$.

The solubility of halides in protic polar solvents like water or aprotic polar solvents such as NMP is high. Halide groups form solvate complexes with a multitude of common organic solvents, thereby introducing further challenges concerning the storage and application of these materials. This is particularly relevant in using HEH as an electrode in incorporation with standard liquid electrolytes or fabricating electrode sheets with conventional dispersion solvents. Handling analytical preparations of HEHs can be considered exceptionally challenging as, with any HEM, the material possesses a complex composition while HEHs additionally have considerable moisture sensitivity. Any commonly employed analytical methods such as scanning electron microscopy (SEM), energy-dispersive X-ray spectroscopy (EDX), electron paramagnetic resonance (EPR), powder X-ray diffraction (PXRD) and single crystal X-ray diffraction (SCXRD) may require various precautions to be made to ensure a HEH does not decompose due to moisture exposure i.e. the usage of capillaries for PXRD or the usage of an inert transfer vessel for SEM and EDX.

Structural Characterization of High-Entropy Halides

Characterizing HEMs, such as HEOs and HEHs, can be very challenging. Established methods for structural analysis of traditional oxides and halides, such as single crystal X-ray diffraction (SCXRD) and powder X-ray diffraction (PXRD), are insufficient due to the chemical and structural complexity of HEM phases. SCXRD only provides information on an average structure therefore, any information on which transition metals are occupying which sites in a crystal lattice is not retained, as the electron density provided by SCXRD is the average for a crystallographic site.[44] Complimentary powder diffraction analysis may yield information on the structure type and if a HEM is single-phase or multi-phase, but no information on the exact composition can be obtained. It is, however, possible to determine qualitatively if a specific element (ionic radii dependent) is introduced in excess into an existing structure.[45] To fully understand the structures of HEMs, various advanced methods, such as X-ray absorption near edge (XANES)[46,47] and extended X-ray absorption fine structure (EXAFS)[46,48,49] experiments, neutron diffraction, in-situ PXRD, and in-situ X-ray absorption spectroscopy (XAS)[46–49] can be used. XAS allows to determine the oxidation state of elements within a HEM, and if conducted *in-situ*, tracking of oxidation state evolution in dependence on operating conditions (temperature, pressure, atmosphere, cycling parameters for electrochemical experiments) is possible.[50]

EXAFS experiments can be conducted to acquire information on the local structure and ordering of HEMs. EXAFS allows investigation into the post-edge absorption spectrum of a material, while XANES investigates the x-ray absorption before the absorption edge (pre-edge). If a structural model of a HEM is obtained utilizing SCXRD, the spectra acquired employing EXAFS and XANES allow the acquisition of information on the local structure of a HEM, i.e. distribution of transition metals at various sites in the crystal lattice.[49] EXAFS allows additional information on the coordination shells of transition metals depending on the position of peaks. Peaks at lower distances from 1–2 Å correspond, for instance, to the scattering of the absorber (i.e. Fe) and first nearest neighbor (i.e. oxygen), while 2–3 Å correspond to the scattering of the absorber to the second nearest neighbor.[49] To fully understand the structure of a HEM, a combinatory approach of advanced methods such as EXAFS/XANES and traditional SCXRD and PXRD is necessary. SCXRD and PXRD will provide a structural model to fit EXAFS/XANES data to refine the structural model and attain site occupation probabilities and coordination.[49] Moreover, it is important to point out that when transitioning from HEOs to HEHs, halides are significantly less stable against moisture. Therefore, most sample preparation and tests must be conducted under inert conditions.

Electrode Applications of High-Entropy Oxides and Halides

Traditional electrode materials such as NMC ($Li[CoMnNi]O_2$)[51,52] Li_xMnO_4[53] or Li_2FeCl_4[11,26] often act as intercalation or insertion cathode while graphite[51] or metallic lithium acts as an anode. Structurally, these cathode materials are commonly found to be one of two options: hexagonal or trigonal layered structures or spinel structures.[51] The diffusion mechanism for Li^+ of the layered structures and spinel structures can be described as a hopping mechanism, as shown in Figure 3 for traditional materials and elaborated for high-entropy materials in Figure 4.

Lithium diffusion in layered- and spinel structures occurs via the vacancy hopping mechanism (Figure 3).[51] For layered hexagonal or trigonal layered structures, Li^+ migrates from an octahedral site through a tetrahedral site to a neighboring unoccupied octahedral site. The adjacent tetrahedral site can either be occupied or unoccupied, wherein an unoccupied tetrahedral site is beneficial to promote Li^+ migration. The Li^+ migration is described as an isolated vacancy hop if all but one adjacent octahedral sites neighboring the tetrahedral site are occupied. Isolated vacancy hops are less favorable and less common for Li^+ diffusion due to strong Li–Li interactions acting as a repulsion, resulting in a narrow migration pathway. The lack of a repulsion in divacancy hops, i.e. where a second adjacent octahedral site is unoccupied, results in a more

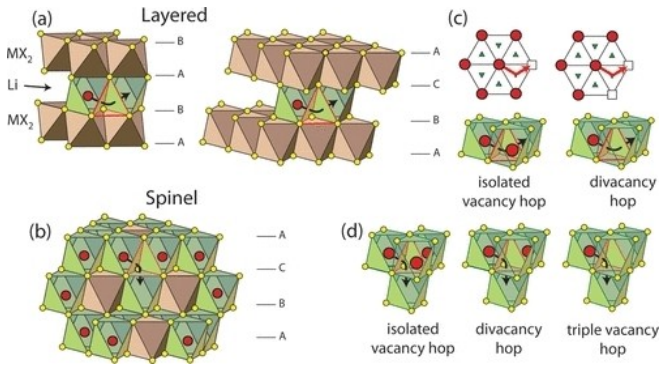

Figure 3. Ionic diffusion mechanisms through Li-Ion hopping in layered (a, c) and spinel structures (b, d) as described by Van Der Ven et al.[51] Reprinted with permission of the American Chemical Society. Copyright © 2013 American Chemical Society.

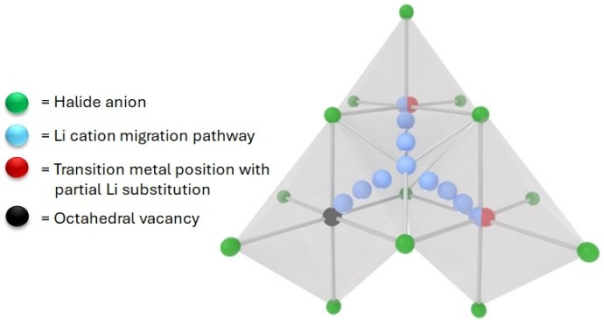

Figure 4. High-entropy effect on a spinel-type structure: Severe lattice distortion due to size mismatches leads to wider migration pathways, partial substitution of Li and (partial) vacancy on tetrahedral sites lead to weaker Li–Li interaction, higher likelihood of vacancies and partial substitution with Li at octahedral sites results in an increased probability for divacancy and triple vacancy hops.

favorable diffusion and, thus, a more probable diffusion process cumulating in achieving higher charge/discharge rates.[51] The Li^+-diffusion mechanism for spinel structures is similar to that of hexagonal/trigonal layered structures. However, a triple vacancy hop is possible within spinel structures, which have even lower energy requirements for migration to occur.[51]

HEOs have been extensively investigated as potential materials for electrode and electrolyte applications. Due to the intrinsically high defect density and structural disorder, mostly because of the multi-cationic content and interactions between different (transition) metal cations, improvements in electrochemical stability as well as significant enhancements of lithium storage capacity and capacity retention, were observed in HEOs materials.[54] The ionic conductivity of HEOs is also enhanced due to the high defect density, which results in a shift towards lower activation energies. The defect hopping mechanism, shown in Figure 3[51] and 4, is greatly enhanced due to the displacement of Li cations onto transition metal positions within a crystal structure.[32] In a traditional system, low-energy and high-energy sites exist. Ion transport can only occur on sites with similar energy levels wherein an overlap of site energy distributions exists. The introduction of cation disorder, i.e., in a HEM, will disrupt high-energy sites and thus lower the energy barrier between Li-occupied sites while raising the energy barrier in low-energy sites. This would result in forming a percolating network of "similar-energy-nearest-neighbor-sites",[32] which would help increase ionic conductivity and diffusion processes in HEMs. Additionally, the energy requirement to perform an isolated vacancy hop in both spinel- and hexagonal/trigonal layered structures highly depends on whether tetrahedral sites are fully occupied, partially occupied, or a vacancy and, if occupied, on the introduced lattice distortion, i.e., on which transition metal resides in the tetrahedral side. Furthermore, in addition to fully vacant sites, partial substitution on both tetrahedral and octahedral sites, which, in a traditional material, would be either fully occupied by transition metals or lithium, lead to overall weaker Li–Li interactions, which may promote the probability of isolated vacancy hops described in Figure 3. For spinel structures, a high degree of lattice distortion and partial vacancy of tetrahedral sites can be induced by the introduction of various lanthanides such as Tb[55] to the crystal structure. The introduction of Lanthanides such as Tb additionally suppresses the formation of a tetragonal phase during cycling while the cubic spinel phase is stabilized, resulting in an overall improvement of cycling stability and rate capability.[55] The enhancement to the diffusion mechanism in spinel-type structures for high-entropy materials can be summarized by multiple effects stemming from a high configurational entropy as shown Figure 4: Lithium displacement onto transition metal positions in a crystal lattice leading to similar-energy sites, lessened Li–Li interaction leading to higher probabilities for isolated vacancy hops and broader migration pathways due to severe lattice distortion leading to an overall increased likelihood of Li^+ diffusion processes in a high-entropy (halide) spinel structure.

For high-entropy fluorophosphate cathodes, commonly used for SIBs such as $Na_3V_{1.9}(Ca,Mg,Al,Cr,Ca)_{0.1}(PO_4)_2F_3$ (HE-NVPF),[56] the discharge plateau at low voltage is promoted, resulting in higher average working voltages of 3.8 V and an increased energy density of 445 $Wh\,kg^{-1}$ while possessing exceptional capacity retention of 80.4% after 2000 cycles at 20 °C. The exceptional enhancements found within high-entropy fluorophosphates can be explained by a lowered migration barrier for sodium ion diffusion in HE-NVPF when compared to traditional p-NVPF, which is a consequence of a high degree of lattice distortion found in high-entropy materials.[56] A recent study on high-entropy metal-organic frameworks (HE-MOFs) for sodium storage[57] revealed that high-entropy effects can affect the electronic structure of a material. Differences in charge density due to the presence of multiple transition metal centers result in an increase of electronegativity for O that enhances electronic conductivity. Increasing entropy in MOF results in a gradual overlap of the valence band and conduction band. Therefore, no forbidden bandwidths exist. This effect facilitates lower insertion energies for Na^+ and allows for high-efficiency charge/discharge cycling.[57] Assuming that Li^+ and Na^+ show great similarities in migration mechanisms, an improvement in capacity retention, cycling stability, and higher average working voltage may be found in both HEOs and HEHs for electrode materials for LIBs.

Table 2. Various traditional and high-entropy materials are used as electrode materials in either lithium-ion batteries (LIBs) or all-solid-state lithium-ion batteries (ASSLIBs) with their specific capacity after a given number of cycles. * = cathode material ** = anode material.

Material	Specific Capacity (mAh/g)	Battery Type	Material class
[CoCuMgNiZn]O[54]	770 after 100 cycles	LIB	HEO**
$Li[Co_{0.33}Mn_{0.33}Ni_{0.33}]O_2$[52]	339 after 50 cycles	LIB	Oxide*
Li_xMnO_4[53]	107.5 after 50 cycles	LIB	Oxide*
$[FeCoNiCrMnCuLi]_3O_4$[58]	500 after 100 cycles	LIB	HEO**
$LiCoO_2$[59]	100 after 10 cycles	ASSLIB	Oxide*
$[CoCuMgNiZn]F_2$[46]	151 after 30 cycles	ASSLIB	HEF*
$[CoCuNiZn]F_2$[46]	106 after 30 cycles	ASSLIB	MEF*
$[CoCuFeNiZn]F_2$[46]	177 after 30 cycles	ASSLIB	HEF*
Li_2FeCl_4[11]	110 after 720 cycles	ASSLIB	Chloride*

Furthermore, entropy stabilization effects found in HEOs used as electrode materials such as $[FeCoNiCrMnCuLi]_3O_4$[58] results in further improvements in cycling stability in that the increase of configurational entropy allows for compensation of enthalpy gain associated with phase separation.[46] HEHs such as $[CoCuFeNiZn]F_2$[46] and $[CoCuMgNiZn]F_2$[46] show increased discharge capacity due to the multi-cationic nature of the HEHs and cycling stability over 30 cycles when compared to both traditional fluorides and medium-entropy fluorides such as $[CoCuNiZn]F_2$.[46] A comparison of various traditional materials, HEOs, HEHs and medium-entropy halides can be found in Table 2.

In accordance with Table 2, HEOs perform significantly better as electrode materials for both LIBs and ASSLIBs when compared to their traditional material counterparts regarding specific capacity. All HEOs and halides in Table 2 also show increased cycling stability over their traditional material counterparts due to the entropy stabilization effect and lattice distortion. Fluorides such as $[CoCuMgNiZn]F_2$[46] show overall high specific capacities with good cycling stability when used as a cathode material in an ASSLIB. Currently, no high-entropy chlorides or bromides have been investigated and used in ASSLIBs. Li_2FeCl_4[11] is, however, a promising traditional chloride spinel structure with promising cycling stability and specific capacity. If the high-entropy concept, which has been so far applied to oxide and a few fluoride electrode materials, is applied to chloride cathodes, it potentially opens a new class of cathode materials for ASSLIBs. As demonstrated above, halides show promising chemical stability paired with good specific capacities and common simple-in-use precursor materials. Halide spinel-type materials could provide a solid foundation for the design of HEHs, which could be used as electrode materials in ASSLIBs due to the availability of precursors, simplicity of doping, and sufficient thermal stability.

Summary and Outlook

This concept illustrates the direction towards a novel electrode material class achieved by implementing a high-entropy approach. Considering the findings from previous studies on HEOs, we propose a comprehensive investigation into the potential of novel high-entropy halide materials, particularly those in the chloride class. We assume that high-entropy halide materials will have increased cycling stability and a broader electrochemical window compared to traditional halide materials, which, for example, may allow faster cycling. This assumption is based on successfully applying the high-entropy concept to HEOs and high-entropy fluorides, yielding increased cycling stability and a broadened electrochemical window. The electrochemically active and stable single-component counterparts, for example, Li_2FeCl_4, provide a solid basis for designing new families of high-entropy halides for electrochemical applications. It is our contention that research in this area will considerably expand the range of suitable electrode materials for batteries, especially solid-state ones.

Acknowledgements

This work was supported by the project of "High-Performance Solid-State Batteries" (HIPSTER) from "Ministerium für Kultur und Wissenschaft des Landes Nordrhein-Westfalen". Open Access funding enabled and organized by Projekt DEAL.

Conflict of Interests

The authors declare no conflict of interest.

Data Availability Statement

Research data are not shared.

Keywords: high-entropy Material · oxides · halides · electrochemistry · electrode

[1] B. Cantor, I. Chang, P. Knight, A. Vincent, *Mater. Sci. Eng. A* **2004**, *375*, 213–218.
[2] J. W. Yeh, S. K. Chen, S. J. Lin, J. Y. Gan, T. S. Chin, T. T. Shun, C. H. Tsau, S. Y. Chang, *Adv. Eng. Mater.* **2004**, *6*, 299–303.

[3] Y. Zhang, T. T. Zuo, Z. Tang, M. C. Gao, K. A. Dahmen, P. K. Liaw, Z. P. Lu, *Prog. Mater. Sci.* **2014**, *61*, 1–93.
[4] C. M. Rost, E. Sachet, T. Borman, A. Moballegh, E. C. Dickey, D. Hou, J. L. Jones, S. Curtarolo, J.-P. Maria, *Nat. Commun.* **2015**, *6*, 8485.
[5] T. Wang, J. Fan, C. L. Do-Thanh, X. Suo, Z. Yang, H. Chen, Y. Yuan, H. Lyu, S. Yang, S. Dai, *Angew. Chem.* **2021**, *133*, 10041–10046.
[6] T. Wang, H. Chen, Z. Yang, J. Liang, S. Dai, *J. Am. Chem. Soc.* **2020**, *142*, 4550–4554.
[7] S. Akrami, P. Edalati, M. Fuji, K. Edalati, *Mater. Sci. Eng. R* **2021**, *146*, 100644.
[8] J. Yan, D. Wang, X. Zhang, J. Li, Q. Du, X. Liu, J. Zhang, X. Qi, *J. Mater. Sci.* **2020**, *55*, 6942–6951.
[9] Z. Lun, B. Ouyang, D.-H. Kwon, Y. Ha, E. E. Foley, T.-Y. Huang, Z. Cai, H. Kim, M. Balasubramanian, Y. Sun, *Nat. Mater.* **2021**, *20*, 214–221.
[10] K. Giagloglou, J. L. Payne, C. Crouch, R. K. Gover, P. A. Connor, J. T. Irvine, *J. Electrochem. Soc.* **2018**, *165*, A3510.
[11] Z. Liu, G. Zhang, J. Pepas, Y. Ma, H. Chen, *ACS Energy Lett.* **2024**, *9*, 5464–5470.
[12] R. Kanno, Y. Takeda, O. Yamamoto, *Mater. Res. Bull.* **1981**, *16*, 999–1005.
[13] S. Yan, S. Luo, L. Yang, J. Feng, P. Li, Q. Wang, Y. Zhang, X. Liu, *J. Adv. Ceramics* **2022**, *11*, 158–171.
[14] M. C. Gao, J.-W. Yeh, P. K. Liaw, Y. Zhang, *High-Entropy Alloys: Fundamentals and Applications*, Springer, **2016**.
[15] Y. Lin, S. Luo, W. Zhao, Q. Sun, J. Cong, P. Li, P. Li, S. Yan, *J. Energy Chem.* **2024**, *98*, 441–471.
[16] Y. Yao, Q. Dong, A. Brozena, J. Luo, J. Miao, M. Chi, C. Wang, I. G. Kevrekidis, Z. J. Ren, J. Greeley, *Science* **2022**, *376*, eabn3103.
[17] T. Ying, T. Yu, Y.-S. Shiah, C. Li, J. Li, Y. Qi, H. Hosono, *J. Am. Chem. Soc.* **2021**, *143*, 7042–7049.
[18] S. Jiang, T. Hu, J. Gild, N. Zhou, J. Nie, M. Qin, T. Harrington, K. Vecchio, J. Luo, *Scr. Mater.* **2018**, *142*, 116–120.
[19] A. Mao, H.-Z. Xiang, Z.-G. Zhang, K. Kuramoto, H. Zhang, Y. Jia, *J. Magn. Magn. Mater.* **2020**, *497*, 165884.
[20] R.-Z. Zhang, M. J. Reece, *J. Mater. Chem. A* **2019**, *7*, 22148–22162.
[21] Q. Wang, L. Velasco, B. Breitung, V. Presser, *Adv. Energy Mater.* **2021**, *11*, 2102355.
[22] N. J. Szymanski, P. Nevatia, C. J. Bartel, Y. Zeng, G. Ceder, *Nat. Commun.* **2023**, *14*, 6956.
[23] M. Itoh, Y. Inaguma, W.-H. Jung, L. Chen, T. Nakamura, *Solid State Ionics* **1994**, *70*, 203–207.
[24] I. Kokal, M. Somer, P. Notten, H. Hintzen, *Solid State Ionics* **2011**, *185*, 42–46.
[25] P. J. Kumar, K. Nishimura, M. Senna, A. Düvel, P. Heitjans, T. Kawaguchi, N. Sakamoto, N. Wakiya, H. Suzuki, *RSC Adv.* **2016**, *6*, 62656–62667.
[26] H. Lutz, A. Pfitzner, J. Cockcroft, *J. Solid State Chem.* **1993**, *107*, 245–249.
[27] E. Dixon, J. Hadermann, S. Ramos, A. L. Goodwin, M. A. Hayward, *J. Am. Chem. Soc.* **2011**, *133*, 18397–18405.
[28] S. Abrahams, J. Bernstein, *J. Chem. Phys.* **1971**, *55*, 3206–3211.
[29] S. Balakumar, S. Ganesa Moorthy, G. Bocelli, C. Subramanian, *Ferroelectrics* **1998**, *207*, 497–505.
[30] A. Cheetham, B. Fender, M. Cooper, *J. Phys. C* **1971**, *4*, 3107.
[31] A. J. Wright, Q. Wang, C. Hu, Y.-T. Yeh, R. Chen, J. Luo, *Acta Mater.* **2021**, *211*, 116858.
[32] Y. Zeng, B. Ouyang, J. Liu, Y.-W. Byeon, Z. Cai, L. J. Miara, Y. Wang, G. Ceder, *Science* **2022**, *378*, 1320–1324.
[33] X. Xu, Z. Shao, S. P. Jiang, *Energy Technol.* **2022**, *10*, 2200573.
[34] R. D. Shannon, *Foundations of Crystallography* **1976**, *32*, 751–767.
[35] K. Y. Tsui, N. Onishi, R. F. Berger, *J. Phys. Chem. C* **2016**, *120*, 23293–23298.
[36] Z. Song, Q. Liu, *Cryst. Growth Des.* **2020**, *20*, 2014–2018.
[37] Q. A. Akkerman, L. Manna, *ACS Energy Lett.* **2020**, *5*, 604–610.
[38] C. Triolo, K. Moulaee, A. Ponti, G. Pagot, V. Di Noto, N. Pinna, G. Neri, S. Santangelo, *Adv. Funct. Mater.* **2024**, *34*, 2306375.
[39] S. Wang, X. Xu, C. Cui, C. Zeng, J. Liang, J. Fu, R. Zhang, T. Zhai, H. Li, *Adv. Funct. Mater.* **2022**, *32*, 2108805.
[40] H. W. Richardson, in *Ullmann's Encyclopedia of Industrial Chemistry*, Wiley – VCH, **2000**.
[41] J. Neuefeind, K. Tödheide, A. Lemke, H. Bertagnolli, *J. Non-Cryst. Solids* **1998**, *224*, 205–215.
[42] H. Podsiadlo, *J. Therm. Anal.* **1991**, *37*, 613–626.
[43] V. L. Cherginets, V. N. Baumer, S. S. Galkin, L. V. Glushkova, T. P. Rebrova, Z. V. Shtitelman, *Inorg. Chem.* **2006**, *45*, 7367–7371.
[44] Y. Waseda, E. Matsubara, K. Shinoda, *X-ray Diffraction Crystallography: Introduction, Examples and Solved Problems*, Springer Science & Business Media, **2011**.
[45] R. E. Dinnebier, S. J. L. Billinge, *Powder Diffraction: Theory and Practice*, The Royal Society of Chemistry, **2008**.
[46] J. Park, Y. Yang, H. Park, A. Sundar, S. Lee, T. L. Kinnibrugh, S.-b. Son, E. Lee, P. Zapol, R. F. Klie, *ACS Appl. Mater. Interfaces* **2024**, *16*, 57151–57161.
[47] P. Ghigna, L. Airoldi, M. Fracchia, D. Callegari, U. Anselmi-Tamburini, P. D'Angelo, N. Pianta, R. Ruffo, G. Cibin, D. O. de Souza, E. Quartarone, *ACS Appl. Mater. Interfaces* **2020**, *12*, 50344–50354.
[48] O. J. Marques, C. Chen, E. V. Timofeeva, C. U. Segre, *J. Power Sources* **2023**, *564*, 232852.
[49] C. M. Rost, Z. Rak, D. W. Brenner, J. P. Maria, *J. Am. Ceram. Soc.* **2017**, *100*, 2732–2738.
[50] N. Schlegel, S. Punke, C. M. Clausen, U. Friis-Jensen, A. F. Sapnik, D. Stoian, O. Aalling-Frederiksen, D. Gautam, J. Rossmeisl, R. K. Pittkowski, *ChemRxiv preprint, DOI: 10.26434/chemrxiv-2024-k1v88*, **2024**.
[51] A. Van der Ven, J. Bhattacharya, A. A. Belak, *Acc. Chem. Res.* **2013**, *46*, 1216–1225.
[52] M. Malik, K. H. Chan, G. Azimi, *Mater. Today* **2022**, *28*, 101066.
[53] H. Tang, Z. Chang, H. Zhao, X.-Z. Yuan, H. Wang, S. Gao, *J. Alloys Compd.* **2013**, *566*, 16–21.
[54] A. Sarkar, L. Velasco, D. Wang, Q. Wang, G. Talasila, L. de Biasi, C. Kübel, T. Brezesinski, S. S. Bhattacharya, H. Hahn, *Nat. Commun.* **2018**, *9*, 3400.
[55] X. Hou, X. Liu, H. Wang, X. Zhang, J. Zhou, M. Wang, *Energy Storage Mater.* **2023**, *57*, 577–606.
[56] Z. Y. Gu, J. Z. Guo, J. M. Cao, X. T. Wang, X. X. Zhao, X. Y. Zheng, W. H. Li, Z. H. Sun, H. J. Liang, X. L. Wu, *Adv. Mater.* **2022**, *34*, 2110108.
[57] X. Xiao, S. Tao, H. Lian, Y. Tian, W. Deng, H. Hou, G. Zou, X. Ji, *ACS Nano* **2024**, *18*, 28444–28455.
[58] C. Duan, K. Tian, X. Li, D. Wang, H. Sun, R. Zheng, Z. Wang, Y. Liu, *Ceram. Int.* **2021**, *47*, 32025–32032.
[59] S. Ohta, S. Komagata, J. Seki, T. Saeki, S. Morishita, T. Asaoka, *J. Power Sources* **2013**, *238*, 53–56.

Manuscript received: December 3, 2024
Revised manuscript received: February 6, 2025
Version of record online: February 21, 2025